http://informahealthcare.com/nan
ISSN: 1743-5390 (print), 1743-5404 (electronic)

Nanotoxicology

Nanotoxicology, 2016; 10(1): 20–31
 DOI: 10.3109/17435390.2014.1000413

informa
healthcare

ORIGINAL ARTICLE

Long-term prevalence of NIRF-labeled magnetic nanoparticles for the diagnostic and intraoperative imaging of inflammation

Jenny Domey[1], Christian Bergemann[2], Sibylle Bremer-Streck[3], Ines Krumbein[4], Jürgen R. Reichenbach[4], Ulf Teichgräber[1], and Ingrid Hilger[1]

[1]Department of Experimental Radiology, Institute of Diagnostic and Interventional Radiology, Jena University Hospital – Friedrich Schiller University Jena, Jena, Germany, [2]Chemicell GmbH, Berlin, Germany, [3]Institute of Clinical Chemistry and Laboratory Diagnostics, Jena University Hospital – Friedrich Schiller University Jena, Jena, Germany, and [4]Medical Physics Group, Institute of Diagnostic and Interventional Radiology, Jena University Hospital – Friedrich Schiller University Jena, Jena, Germany

Abstract

Inflammation is a very common disease worldwide. In severe cases, surgery is often the method of choice. Today, there is a general need for the implementation of image-based guidance methodologies for reliable target resection. We investigated new near infrared fluorescence (NIRF)-nanoparticles (NPs) as a simple but effective bimodal magnetic resonance imaging (MRI) and optical contrast agent for diagnosis and intraoperative imaging of inflammation. Physicochemical analysis revealed that these NPs were highly fluorescent with similar characteristics like unlabeled NPs (hydrodynamic diameter about 130 nm and zeta potential about −10 mV). NP-uptake and NIR-dye labeling was biocompatible to macrophages (no impact on cellular ATP and reactive oxygen species production). These cells could successfully be tracked with MRI and NIRF-optical imaging. I.v. injection of fluorescent NPs into mice led to highly specific T_2-weighted signal of edema due to uptake by phagocytic cells and subsequent migration to the site of inflammation. NIRF signals of the edema region were well detectable for up to 4 weeks, underlining the potential of the NPs for systematic planning and flexible time scheduling in intraoperative applications. NPs were degraded over a time period of 12 weeks, which was not altered due to inflammation. Redistribution of iron might be primarily due to inflammation and not to the presence of NPs per se in a concentration suitable for imaging. Our findings highlight the potential of the NPs to be used as a suitable tool for pre- and intraoperative imaging of inflammation.

Keywords

Biocompatibility, biodistribution, degradation, MRI, optical imaging

History

Received 10 November 2014
Revised 15 December 2014
Accepted 15 December 2014
Published online 17 February 2015

Introduction

Chronic inflammation is known as an inductor for the genesis of numerous chronic illnesses like autoimmune and neurodegenerative disorders and is also a promoter for tumor development (Khatami, 2009; Philip et al., 2004). To avoid secondary diseases, the need for surgical guidance is high in severe cases of inflammation. Although chronic and relapsing inflammation processes are described for diseases requiring surgery, development and characterization of bimodal contrast agents, which are applicable during inflammation are rare. At the same time, diagnosis and surgery remains a frequent and necessary incidence in patients with disorders of the gastrointestinal tract like inflammatory bowel disease (IBD) (Cummings & Rubin, 2006). Furthermore, removal of chronic inflammable tissue is important because it represents a high risk factor of cancer (Schwartsburd, 2003). For this purpose, the development of a simple and biocompatible but effective nanomaterial for diagnostic and surgical approaches would be helpful to assist pre- and intraoperative imaging.

In recent years, multimodal new near infrared fluorescence (NIRF)-labeled particles have been applied for *in vitro* and *in vivo* imaging in several approaches (Jaffer et al., 2009; Sharma et al., 2012). A variety of studies focuses especially on tumor-targeting nanostructures for molecular imaging (Chen et al., 2010; Cheng et al., 2012; Yang et al., 2012). There are also different approaches for detecting inflammation markers as well as nanomaterials that combine magnetic resonance imaging (MRI) and NIRF imaging including active targeting of inflammation markers like VCAM-I (Chen et al., 2010; Jarrett et al., 2008; Koktysh et al., 2011; Lee et al., 2012; Mackay et al., 2011; Nahrendorf et al., 2006; Radermacher et al., 2009; Rimkus et al., 2012; Stoll et al., 2012; Tsourkas et al., 2005). These bimodal nanomaterials might have the potential to combine MRI-based diagnosis and NIRF-associated intraoperative imaging. However, due to their complexity, antibodies and fluorescent dyes bound to the surface of these nanostructures bear the risk of cross-reactivity with tissues and proteins. Unfortunately, detailed studies about biocompatibility and degradability of these materials are often

Correspondence: Ingrid Hilger, Department of Experimental Radiology, Institute of Diagnostic and Interventional Radiology, Jena University Hospital – Friedrich Schiller University Jena, Erlanger Allee 101, 07747 Jena, Germany. Tel: +49 (0)3641 9325921. Fax: +49 (0)3641 9325922. E-mail: jenny.domey@med.uni-jena.de (J. Domey); ingrid.hilger@med.uni-jena.de

missing. Hence, until now there is no clinical approval for bimodal contrast agents combining MRI (diagnosis) and NIRF (intraoperative imaging). Considering the transferability of NP formulations to the clinics, important issues are the characteristics of the nanomaterials' long-term biodistribution and their detectability, which are essential for both diagnosis and operation because they are not often directly successive in time.

For this purpose, we present innovative bimodal NPs with a focus on both successful detection of inflammation during preoperative screening allowing anatomical localization of the diseased area (via MRI) and its subsequent identification during intraoperative surgery (via highly sensitive NIRF-optical imaging) following one single application procedure only. Since cells of the mononuclear phagocytic system (MPS) are strongly participating in the development of inflammation processes, we focused our study on the characterization of innovative fluorescent-labeled iron oxide NPs being used for passive targeting of mononuclear cells. To improve biocompatibility of the magnetic core and NIRF-dye our newly designed NPs are completely coated by a starch matrix. We hypothesize that due to the starch coating the NIR-fluorochrome does not interact with the surroundings and therefore does not alter its physicochemical properties, cellular uptake and biocompatibility compared to non-labeled NPs. *In vitro* investigations of the cellular ATP-level and the production of reactive oxygen species (ROS) in murine macrophages were performed to evaluate potential side effects of the bimodal contrast agent. The analysis of the NP behavior *in vivo* is decisive for consideration to clinical applications. Therefore, we analyzed the long-term detectability within the region of inflammation, organ biodistribution and degradability of the nanoparticulate contrast agent with special focus on the influence of inflammation.

Methods

Characterization of NIR-dye IR780 and synthesis of fluorescent labeled magnetic NPs

The superparamagnetic fluorescent NPs (nano-screenMAG/IR780-D) and the non-fluorescent counterpart (fluidMAG-D) were obtained from chemicell GmbH (Berlin, Germany). Both NPs were synthesized by converting an acidic iron (II/III) salt solution into iron (II/III) carbonate by adding equivalent amounts of alkaline carbonate, followed by a successive thermic reaction to iron (II, III) oxide. The resulting multidomain magnetite (Fe_3O_4) nanocrystals were washed several times with double distilled water and treated with ultrasound to remove unreacted and not tightly bound material.

To obtain fluorescent NPs, these iron oxide cores were enveloped subsequently by the lipophilic near-infrared dye IR780 (IR780-iodide, Sigma-Aldrich, Hamburg, Germany) by means of a desolvation procedure. Again, the particles were washed as described above.

Afterwards, both NP types were coated with soluble starch by means of chemisorption, washed as described above and adjusted to a hydrodynamic diameter of 150 nm. The particle suspension was adjusted to a volume weight of 50 mg/ml and was autoclaved at 121 °C for 20 min immediately afterwards. Autoclaving did not alter the hydrodynamic diameter. A schematic design of both NP types is represented in Figure 1(A).

The spectroscopic features of the dye IR780 and IR780-labeled NPs were determined by absorption and fluorescence measurements after dilution of IR780 in pure ethanol or in double distilled water in case of the bimodal NPs. The absorption spectrum was measured by using an UV/visible spectrophotometer (Ultrospec 4300 pro, GE Healthcare, München, Germany). The fluorescence spectrum was recorded by a spectrofluorometer (FP-6200, Jasco, Gross-Umstadt, Germany) while exciting at 730 nm.

Physico-chemical analysis of fluorescent magnetic NPs

To assess the influence of serum proteins in medium on the hydrodynamic diameter and zeta potential of a NP, a photon correlation spectrometer (Zetasizer Nano-ZS, Malvern Instruments, Herrenberg, Germany) was used. Prior to the measurements, NPs were diluted in deionized water or Dulbecco's modified Eagle medium (DMEM)+10% FCS to a final particle concentration of 0.05 mg/ml. NPs diluted in medium with serum were incubated for 24 h at 37 °C in a 5% CO_2 atmosphere and subsequently spun at maximal speed for 30 s. Supernatant was removed and NPs were gently re-suspended in deionized water. Dynamic light scattering data were recorded and averaged over five measurements. Each measurement was performed for 2 min at 25 °C and with a cuvette measuring position of 4.65 mm. The mean hydrodynamic diameter was recorded as the average of five measurements (*Z*-average). Zeta potential measurements were performed in three measurements, each with 10 runs at 25 °C to provide an average value.

To evaluate differences of the specific surface area of unlabeled NPs and dye-labeled NPs a Nova 2002 instrument (Quantachrome, Odelzhausen, Germany) was used. Surface area was calculated with five data points according to the BET method. Nitrogen adsorption was recorded at 77 K for relative pressure (p/p_0) in the range of 0.06–0.3 after drying by means of a rotary evaporator at 60 °C. Before BET determination, the powder was dried a second time for 2 h at 50 °C under vacuum with the Nova 2002 heating station.

NIR-fluorescence characterization of free lipophilic dye IR780 and IR780-labeled NPs

The NIRF-detectability of fluorescent NPs was assessed by NIR-imaging and compared to control NPs with no dye labeling. For this purpose, NPs were diluted in deionized water (Fe concentration 1 µg/ml) and recorded with an optical NIRF small animal imager (Maestro™, Cambridge Research & Instrumentation, Inc. (CRi), Woburn, MA) using the NIR-filter set for excitation and emission (Ex. 710–760 nm and Em. 800 nm longpass).

Cell culture

To elucidate the impact of NPs on potential target cells, the murine macrophage cell line J774A.1 (CLS Cell Lines Service GmbH, Eppelheim, Germany) was cultured in DMEM/F-12 (1:1) (+)-L-glutamine (Gibco, Darmstadt, Germany) containing 10% fetal calf serum (FCS; Gibco) at 37 °C in a 5% CO_2 atmosphere. When confluency reached approximately a value of 80%, cells were harvested by scraping and used for further experiments as described below.

Determination of metabolic impact of NPs on cells via ATP assay

To investigate the effect of NP-dye labeling on the metabolism of murine macrophages cellular ATP-levels was determined via the ATP assay. In this context, 1.7×10^4 J774A.1-cells/cm^2 were seeded into a 96-well plate and incubated for 24 h. Culture medium was replaced by NP suspensions in cell culture medium (Fe concentration from 0.1 to 50 µg/ml). Untreated cells served as a control for normal metabolic activity and received fresh medium instead of NP solution. DMSO (5%) in DMEM was used as a positive control for cell death. After 4, 24 or 48 h of incubation with the NP (fluorescent and nonfluorescent), the culture medium was removed and cells were washed four times with fresh cell culture medium. Subsequently CellTiter-Glo® Luminescent Cell Viability Assay (Promega, Mannheim, Germany) was performed

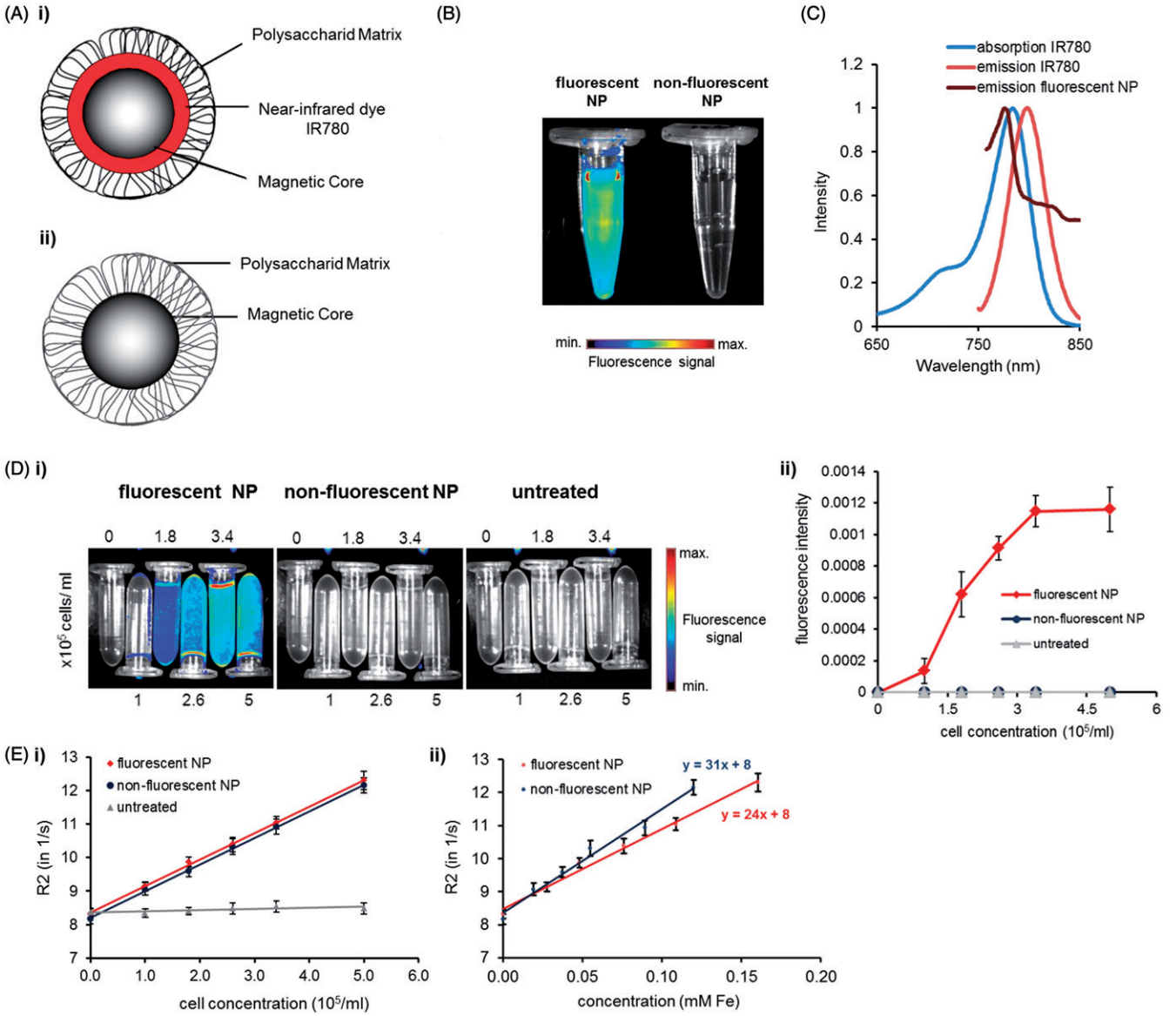

Figure 1. Characterization of fluorescent and nonfluorescent NPs and dye IR780. (A) Scheme of (i) fluorescent and (ii) nonfluorescent NPs. (B) NIRF-imaging of fluorescently labeled and nonfluorescent NPs diluted in deionized water. In contrast to nonfluorescent NPs fluorescently labeled NPs show a detectable NIR fluorescent signal. (C) Spectral analysis of free lipophilic dye IR780 dissolved in ethanol and IR780-labeled NPs diluted in double-distilled water. (D–E) Image-based detection of NP-labeled murine macrophages (J774A.1-cells) embedded in 1% agarose *in vitro*. (D) Fluorescence and (E) MR imaging (at 1.5 T). (D) (i) Intensity scaled NIRF-images and (ii) fluorescence signaling of NP-treated cells. (E) R_2-relaxation rates of (i) fluorescent and nonfluorescent NPs in macrophages and (ii) related to the cellular iron content.

as previously described (Hoskins et al., 2012). Luminescence intensity was measured via LUMIstar Galaxy (BMG LABTECH GmbH, Ortenberg, Germany). Data were given as relative values to untreated controls, which was set to be 100% viable. All experiments were repeated at least four times with six parallels each.

Determination of NP-mediated production of reactive oxygen species

To analyze the influence of NP-uptake on the production of ROS, which are mainly produced by macrophages in terms of an immune reaction, the ROS-level of the macrophages was investigated using a ROS-Assay-Kit (OxiSelect™ Intracellular ROS-Assay Kit, CELL BIOLABS, Inc., BIOCAT GmbH, Heidelberg, Germany). Hereto, J774A.1-cells were seeded at $1.4 \times 10^6/cm^2$ in a 96-well plate. After incubation for 24 h, cells were exposed to increasing concentrations of the NP (Fe concentration ranging from 0.1 to 50 µg/ml) suspended in culture medium. After 4, 24 or 48 h of incubation, cells were washed three times with HBSS and incubated for further 45 min in the presence of 100 µM nonfluorescent DCFH-DA in culture medium protected from light. Cells were washed three times with HBSS and subsequently lysed with 1% triton X-100 in HBSS (100 µl/well). The fluorescence intensity of ROS oxidized 2′,7′-dichlorodihydrofluorescein (DCF) of the samples was measured at 530 nm after excitation at 480 nm using a microplate fluorescence reader (TECAN infinite M200, TECAN, Crailsheim, Germany). The percentage of fluorescent DCF was set in relation to untreated control cells. The experiment was performed in triplicates with four parallels each.

Fluorescence microscopy of NPs in murine macrophages

To examine the influence on uptake and localization of fluorescence labeling of NPs in murine macrophages 2×10^4 J774A.1-cells were seeded onto chamber slides. Twenty-four hour later, cells were washed twice with HBSS. Fluorescent NPs were added to the cells (final Fe concentration of 25 µg/ml). As a control for

the influence of dye labeling nonfluorescent NP suspended in cell culture medium or cell culture medium without NPs were added to the cells. After incubation for 24 h, cells were washed three times with HBSS and fixed with 4% formaldehyde. Nuclei of the cells were stained with Hoechst 33258 (Applichem, Darmstadt, Germany). The uptake and localization of the fluorescing NP into the cells was investigated by fluorescence microscopy with EVOS fl (PEQLAB, Erlangen, Germany) using the light cubes DAPI and Cy7.

Detection of NPs in murine macrophages via macroscopical fluorescence reflectance and MR-imaging

To study the spectroscopic and magnetic properties of fluorescent NPs for optical and MR-imaging after uptake by murine macrophages, J774A.1-cells (1×10^6) were grown in cell culture flasks ($25\,cm^2$) for 48 h. Subsequently, cells were treated with fluorescent or nonfluorescent NPs in a concentration of 50 µg/ml Fe in cell culture medium. Control cells received culture medium instead of NP solution. After 24 h of incubation medium was removed and cells were harvested by scraping. After washing the macrophages with HBSS by centrifugation three times to remove NPs, cells were fixed with 4% formaldehyde in HBSS solution. Increasing macrophage concentrations (0, 1, 1.8, 2.6, 3.4, 5×10^5 cells/ml) were gently suspended into 60 °C warm agarose (final concentration 1% w/v) placed in 2 ml reaction tubes to simulate tissue properties. These agarose phantoms were cooled down for 2 min on ice to solidify agarose quickly to keep cell concentration consistent and to avoid accumulation of cells at the bottom of the tubes. The spectroscopic properties of phantoms with NP-treated cells were determined by using a whole body NIRF small animal imager (Maestro™, Cambridge Research & Instrumentation, Inc. (CRi)) using the NIR-Filter set for excitation and emission (Ex. 710–760 nm and Em. 800 nm longpass). To assess the magnetic properties of the NP's iron oxide core, the same samples were measured using a 1.5 T MRI scanner (MAGNETOM Avanto, Siemens, München, Germany) at room temperature. To calculate the relaxivities r_1, r_2 and r_2* of NP, the iron content in the cells was quantitated by flame atomic absorption spectrometry as previously described (Rimkus et al., 2011).

Animals

Ten-week-old male NMRI mice (37–49 g) (Elevage Janvier, Le Genest Saint Isle, France) were housed under standard conditions with food and water ad libitum. All procedures were approved by the regional animal committee and were in accordance with international guidelines on the ethical use of animals. To reduce tissue auto-fluorescence 7 days prior and during the whole experiment, mice were fed with a special diet consisting of food low in manganese (C 1039 Altromin, Lage, Germany). During the imaging experiments mice were anesthetized using oxygen with 2% isoflurane (Actavis, Germany).

NIRF-optical imaging and biodistribution of NPs in edema bearing mice

Mice were shaved in the abdominal region 24 h before each experiment. To detect fluorescent-labeled NPs in the region of inflammation mice were treated with 1% zymosan A to induce edema at the right hind leg. As a control for edema development mice were subcutaneously injected with physiological NaCl solution at left hind leg. For NIRF optical imaging of phagocytic cells in the edema region, fluorescent NPs were injected with a dose of 40 µmol Fe/kg body weight ($n = 5$) via the tail vein. To ensure specific NIR-signaling of fluorescence dye-coupled NPs, nonfluorescent NPs ($n = 6$) or physiological NaCl solution ($n = 4$) were injected as a control into further groups of edema bearing mice. The progression of inflammation was documented (0, 2, 4, 5, 6, 7 and 8 h post injection (p.i.) of both NPs or NaCl) using the whole body optical NIRF small animal imager (see above). To confirm that monocyte migration after NP uptake is related to the development of inflammation, a further group of NMRI-mice ($n = 3$) was treated twice a day with methylprednisolone (Urbason solubile, Kohlpharma GmbH, Merzig, Germany) up to 48 h before and immediately after edema induction. Methylprednisolone-treated mice were injected with fluorochrome labeled NP and observed up to 8 h p.i. with the whole body optical NIRF small animal imager. In addition, to confirm that the fluorescent signal emerges from fluorescently labeled macrophages to the edema region, bone marrow derived macrophages (BMDMs) from NMRI mice were obtained by *in vitro* differentiation, labeled with nano-screenMAG/IR780-D and subsequently injected via the tail vein into a further group of NMRI mice ($n = 3$) using a previously described protocol (Naha et al., 2010). NIR-fluorescence signals were monitored up to 48 h for both groups. To assess the biodegradability of fluorescent NPs, the long-term biodistribution of the bimodal NPs in the edema region and in organs of NMRI-mice was examined 24 and 48 h, as well as 1, 4, 8 and 12 weeks p.i. via fluorescence imaging with the optical NIRF small animal imaging system. To analyze effects of the inflammation state on NP biodistribution, a further group of untreated animals was injected with fluorescent NP and investigated at 24 h, 4 weeks and 12 weeks after NP application ($n = 4$). For semi-quantitative analysis of the specific fluorescent signals, regions of interest (ROIs) were selected on the hind leg edema region and an average signal (scaled counts per second) was recorded for each documented time point.

MR-imaging of bimodal NPs in edema bearing mice

To confirm that fluorescently labeled NPs reveal also MR-detectability edema induction and bimodal NP treatment was performed with NMRI-mice as described above ($n = 3$). Control mice received NaCl-solution instead of NPs ($n = 3$). The accumulation of NPs within the edema region was investigated 8 h p.i. with a 3 T MRI scanner (MAGNETOM Trio, Siemens) using a small animal coil and a T_2-weighted, 3D SPACE sequence. Signal intensities of edema regions were analyzed using T_2-weighted images of NP- and NaCl-treated mice by selecting ROIs to cyst and proteinous liquid core of edemas. The corresponding signal changes were determined relative to signals of the edema surrounding muscle tissue.

Determination of iron content in organs of healthy and edema bearing mice after NP treatment

To investigate long-term biodistribution and to quantify NP uptake and degradation after application, iron content of organs as well as at the site of inflammation of healthy and edema bearing NMRI-mice was verified (24 h, 4 and 12 weeks after i.v. NP application). Organs were removed and dried at 40 °C for 48 h. The tissues were weighted, digested with HNO_3 and $HClO_4$ and subsequently heated at 70, 160 and 260 °C for 1 h. To solve iron oxide, deposits were taken up in HNO_3 and flame atomic absorption spectrometry was performed to determine iron content of samples as previously described (Rimkus et al., 2011). Mice receiving only sodium chloride instead of NPs were used as controls for the natural existing iron amount in organs.

Histological analyses of murine organs after edema induction and NP treatment

Prussian blue staining was performed to detect and localize NPs in terms of trivalent iron within cells of organ tissues after

application in edema bearing mice. For this purpose, organs of mice were dissected at 24 h, as well as 4 and 12 weeks after injection of NPs or NaCl solution and finally fixed for 24 h using a neutrally buffered 5% methanol/formaldehyde solution and subsequently rinsed with PBS. The organs were embedded in paraffin and cut into slices. Tissue slices were treated for 5 min with 10% potassium ferrocyanide(II)trihydrate solution. Subsequently, slides were incubated for 30 min with 5% potassium ferrocyanide(II)trihydrate in a 10% HCl solution, washed and counter-stained for 3 min with nuclear fast red (Roth, Karlsruhe, Germany). Organ slices were examined by light microscopy (Olympus BX50, Olympus, Hamburg, Germany) to determine iron distributions within organs.

Assessment of transferrin levels in blood via ELISA

Blood from healthy or edema bearing NMRI-mice was collected by cardiocentesis 24 h, 4 or 12 weeks after i.v. application of either nsIR780-D NP, fluidMAG-D NP or NaCl solution. Blood was centrifuged for at least 4 h at 4 °C and 1500×g and subsequently serum was collected. Serum samples were used for sandwich ELISA. For plate coating a capture antibody (Transferrin Chicken anti-Human polyclonal Antibody, LSBio, Seattle, WA, diluted 1:500 in PBS) was used. Murine serum was diluted in PBS (pH 7.2) (1:200 000) and added to the wells and subsequently incubated over night at 4 °C. To calculate transferrin concentrations, a transferrin standard (transferrin protein from mouse, Fitzgerald, Acton, MA) was applied. For transferrin detection a horse raddish peroxidase (HRP)-conjugated detection antibody (Transferrin Goat anti-Mouse polyclonal (HRP) Antibody, LSBio) was used (1:1000). As a substrate for HRP, orthophenylenediamine was added to phosphate citrate buffer (pH 5.0) and 30% H_2O_2 which was added to the plates. Enzymatic reaction was stopped via adding 1.5 M H_2SO_4. The absorption of the samples in the wells was measured at 492 nm. The experiment was repeated three times.

Statistical analysis

Data are represented as means ± standard error. Excel or Sigma Plot was applied for statistical analysis by using the two-tailed Student's t test. Calculated p values of 0.05 or less were considered statistically significant.

Results

Physico-chemical characterization of fluorescence labeled iron oxide NPs

Our data show that in contrast to unlabeled control NPs (Figure 1A) fluorescence (IR780) labeled NP were detected *in vitro* by using optical imaging via NIRF small animal imaging (Figure 1B). The fluorescent NPs showed a specific signal which could be detected very well using specific NIR-filter sets (see Methods section). These observations were in agreement with the spectroscopic properties of free lipophilic fluorescent dye IR780 showing an excitation maximum of 784 nm and an emission maximum at 798 nm which was slightly shifted to a fluorescence maximum at ca. 776 nm when IR780 dye envelopes the iron oxide cores of the NPs (Figure 1C). Consequently, fluorescent NPs were effectively labeled with IR780 and applicable for further *in vitro* imaging experiments.

The physicochemical analysis showed that both the fluorescent and unlabeled NPs possessed a comparable hydrodynamic diameter around 130 nm (134 and 129 nm), which was more than doubled for both particles after 24 h incubation in medium with 10% serum (Table 1). Furthermore, both particle types exhibited a slightly positive zeta potential (8.1 and 10.5 mV) (Table 1).

Table 1. Physicochemical characterization of fluorescent and nonfluorescent NPs.

NP	Size [nm]	Polydispersity index	Zeta potential (mV)	Specific surface area (m^2/g)
Fluorescent NPs[a]	134 ± 1.3	0.108 ± 0.011	8.1 ± 0.3	24.2
Non-fluorescent NPs[a]	129 ± 0.6	0.112 ± 0.013	10.5 ± 0.4	14.8
Fluorescent NPs[b]	320 ± 108	0.285 ± 0.12	−29 ± 1.2	–
Non-fluorescent NPs[b]	344 ± 30	0.423 ± 0.11	−28 ± 1.5	–

Size, zeta potential in deionized water and after 24 h incubation in DMEM + 10% FCS and specific surface area.
[a]Deionized water.
[b]After 24 h incubation in DMEM + 10% FCS.

Table 2. Determination of relaxivities r_1, r_2 and r_2* for NP after cellular uptake at 1.5 T, 25 °C.

NP	r_1 [$M^{-1}s^{-1}$]	r_2 [$M^{-1}s^{-1}$]	r_2* [$M^{-1}s^{-1}$]
Fluorescent NPs	0.36	24	797
Non-fluorescent NPs	0.42	31	993

This finding is due to the presence of starch on the surface of the NPs, which is considered to exhibit a neutral charge which turns into a negative one after 24 h incubation with DMEM + 10% FCS (−29 and −28 mV). Thus, there are no modifications in size and zeta potential of the NPs after labeling with strongly positively charged fluorescent dye IR780. The characterization of the specific surface area of the NP revealed that fluorescent NPs exhibit a slightly larger surface area than nonfluorescent NPs (24.2 and 14.8 m^2/g) (Table 1).

Optical and MR imaging properties of bimodal NPs in murine macrophages *in vitro*

Embedded in 1% agarose, only J774A.1 cells marked with fluorescent NPs showed specific NIRF-signaling due to IR780-labeling of these particles (Figure 1Di). Increasing concentrations of fluorescent NP-labeled cells in agarose led to a higher average fluorescence signal up to 0.001 fluorescence units, confirming consistent NIR-imaging of these NPs also after uptake into cells (Figure 1Dii). In contrast, unlabeled macrophages and cells internalizing unlabeled NPs were not detected by NIR-fluorescence imaging.

Investigations on the magnetic properties of our bimodal NPs indicated that labeling of macrophages led to an increased R_2 relaxation rate (=$1/T_2$) in contrast to untreated cells (for all tested cell concentrations around $R_2 = 8.5\,s^{-1}$) (Figure 1Ei). Increasing the NP-loaded cell concentrations in the samples resulted in even stronger T_2 shortening and a higher relaxation rate of labeled cells for fluorescent and nonfluorescent NPs ($R_2 = 12.3\,s^{-1}$and $R_2 = 12.2\,s^{-1}$) compared to untreated control cells. Even the lowest concentration of NP-marked cells tested (1×10^5 cells/ml), where cells had similar labeling intensities, revealed a stronger T_2 shortening than untreated cells ($R_2 = 9.14\,s^{-1}$ for fluorescent and $R_2 = 9.07\,s^{-1}$ for nonfluorescent NPs). The determination of the r_2-relaxivities of the NPs within J774A.1 cells embedded in 1% agarose resulted in 24 $mM^{-1}s^{-1}$ for bimodal and 31 $mM^{-1}s^{-1}$ for nonfluorescent NPs (Figure 1Eii). Overall, the calculation of the relaxometric properties revealed slightly lower r_1, r_2 and r_2* relaxivities for labeled compared to the unlabeled control NPs after uptake into cells (Table 2). Thus, the labeling of magnetic NPs with fluorescence dye appeared to have only marginal effects on MR relaxation.

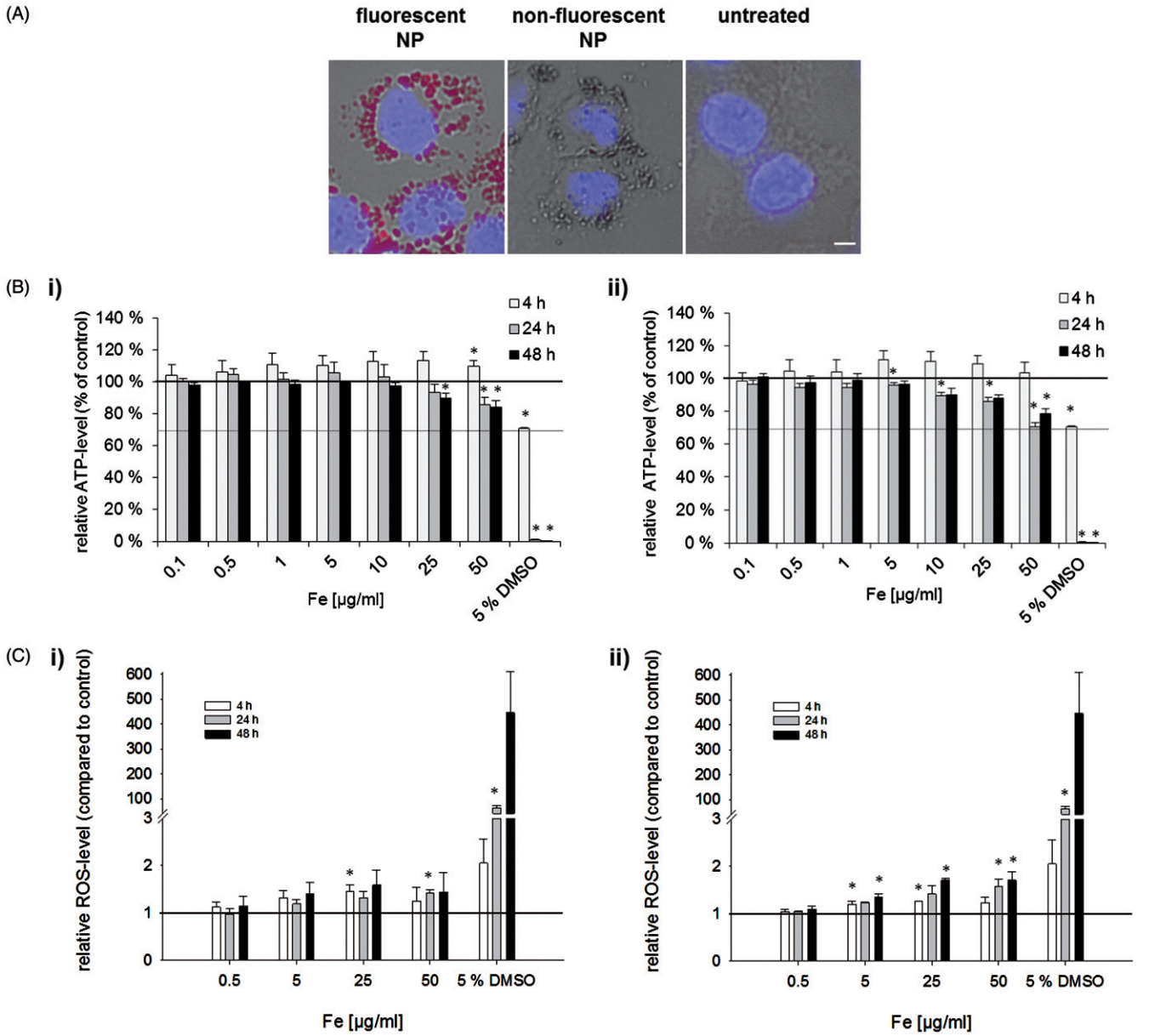

Figure 2. Effect of fluorescent and nonfluorescent NPs on metabolic activities in murine macrophages. (A) Uptake of NPs in J774A.1-cells after incubation with NPs (25 µg Fe/ml, 24 h). Scale bar: 50 µm. (B) Relative ATP-level of J774A.1 cells. Cells incubated with increasing concentrations of (i) fluorescent (ii) or nonfluorescent NP. Relative was ATP-level normalized to untreated control cells (ATP-production $\hat{=}$ 100%), cell death positive control: 5% DMSO. Four independent experiments with six repetitions each were performed. (C) Effect of fluorescent NPs on ROS production in J774A.1 cells after incubation with (i) fluorescent (ii) or nonfluorescent NPs. ROS-level was normalized to the ROS production of untreated control cells (ROS production level $\hat{=}$ 1), positive control for ROS production: 5% DMSO. Three independent experiments with three repetitions each were performed. Results are represented as mean values ± standard error of mean compared to untreated control cells. $^*p \leq 0.05$.

Uptake of bimodal NPs into macrophages

Microscopic evaluations of the uptake of fluorescent NPs showed that J774A.1 macrophages internalized the bimodal NP formulation as well as the mono-modal counterpart to a similar extent (Figure 2A). NIR-fluorescence signaling was shown to be specific for phagocytized bimodal NPs. Both particles exhibited a similar intracellular distribution and were located around the nuclei of J774A.1-cells. Untreated macrophages did not show any particle accumulation. Consequently, the presence of the NIR-dye does not alter internalization behavior into macrophages.

Bimodal NPs are harmless to murine macrophages *in vitro*

To determine the metabolic impact of fluorescently labeled NPs on macrophages, the relative ATP-level of target cells was tested. Fluorescently labeled and nonlabeled NPs showed similar effects on cellular ATP-levels over time. Overall, they had no significant effect on changing cellular ATP-levels after 4 h co-incubation with macrophages (Figure 2B). However, regardless of NIRF-labeling only a slight decrease of ATP-levels was found 24 and 48 h after incubation of NPs on J774A.1-cells compared to untreated control cells. In summary, bimodal NP treatment was harmless to macrophages even at the highest NP concentration tested (50 µgFe/ml, cell viability > 70% according to DIN EN ISO 109935).

Bimodal NPs do not enhance production of ROS by macrophages *in vitro*

A similar behavior concerning ROS production within J774A.1-cells was observed for NIR-fluorescent and nonfluorescent control NPs. There was only a slight increase of ROS production

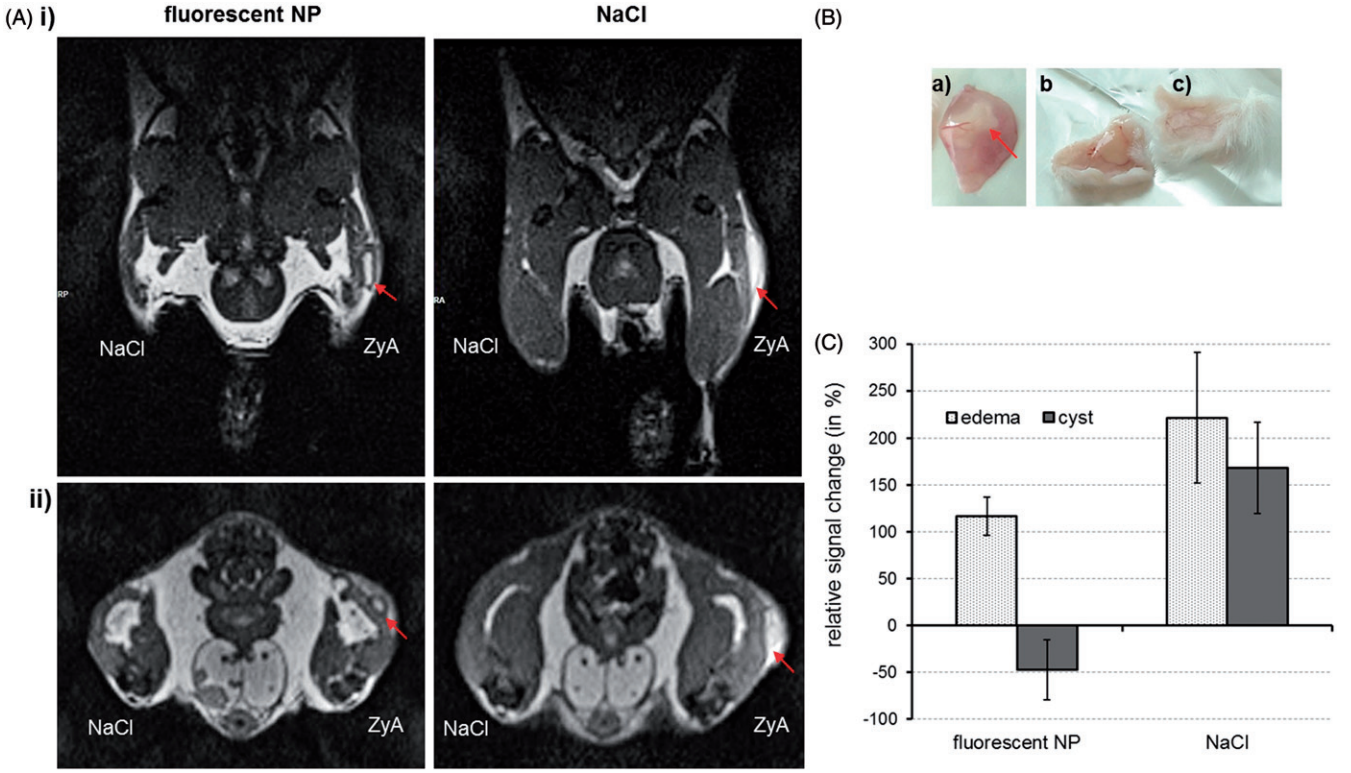

Figure 3. MRI of mononuclear phagocytic cells in hind leg edema with fluorescent NPs in NMRI-mice. Subcutaneous edema was induced at right hind leg using 1% zymosan A solution (ZyA). NaCl-solution injected s.c. at left hind leg served as a control for edema development. Fluorescent NPs were injected i.v. in edema bearing mice (40 µmol Fe/kg bw). NaCl solution (control of NP signal) was injected to a further group of edema bearing mice. The NP distribution was documented 8 h p.i. with 3 T MRI. (A) T2-weighted MR-images of hind leg edema bearing mice treated with either fluorescent NPs (left) or NaCl solution (right) in (i) longitudinal or (ii) transverse view. The arrows show the bright cyst of edema which can clearly be distinguished from the rest of edema only after NP accumulation (NPs represent a dark region around edema cyst) (B) Dissection of edema region. (a) The edema consists of a cyst (arrow), which is filled with pus and surrounded by proteinous liquid. (b) Skin of edema side (after s.c. zymosan-injection) exhibiting glossy proteinous liquid and (c) skin of control site (after *s.c.* NaCl-injection). (C) Relative signal changes which were determined from the T_2-weighted images by using muscle tissue as reference signal.

in J774A.1 cells treated with increasing NP concentrations over a time period of 48 h (Figure 2C). For both particle variants, a maximum increase of approximately 1.5-fold ROS production compared to the untreated control cells was found. Thus, ROS production of macrophages was not strongly increased by the incubation with the tested iron oxide NPs.

Detection of bimodal NPs in murine macrophages *in vivo* in edema regions of mice

In vivo magnetic resonance tracking of the bimodal NPs revealed an enhanced T_2-weighted signal of the fluorescent NPs within the hind leg edema region of mice 8 h p.i. (Figure 3Ai and ii). In contrast to the control mice receiving NaCl solution instead of NPs, the edema could be clearly identified by discriminating the cyst between the inner pus and the proteinous liquid surrounding the edema region (Figure 3Ai, Aii and B). More precisely, a negative signal change (up to −50% compared to surrounding muscle tissue) within the edema region was seen for the mice injected with fluorescent NPs due to their accumulation within the cyst which led to an MR-signal decrease (Figure 3C). In contrast, NaCl-treated animals revealed similar positive signal changes in the edema region (inner pus) and cyst (>150% compared to the surrounding muscle tissue). Thus, bimodal NPs cause signal changes on T_2-weighted images and allow for differentiation of cellular compartments and liquids of the edema region making them suitable for preoperative MR-screening.

Investigations of the *in vivo* NIRF-imaging quality of our fluorescence-labeled NPs demonstrated that they were specifically accumulating within edema regions of mice after i.v. application. Fluorescence of labeled NPs could be initially detected 2 h p.i. within the edema region at the hind leg with a continuous enhancement of fluorescence intensity thereafter (Figure 4Ai). The fluorescence signal peaked at 48 h p.i. (Figure 4i and ii). In comparison, mice receiving methylprednisolone before injection with bimodal NP (to verify the inflammation state) revealed significantly ($p < 0.05$) lower fluorescence signals within the edema region at 4, 6, 7 and 8 h after injection of NPs (Figure 4ii). During an observation time of 8 h after zymosan induction and NP treatment, the fluorescence intensity in methylprednisolone treated animals was approximately half compared to the one observed in animals without inhibition of inflammation. In addition, edema bearing animals which were injected with bimodal NP-labeled BMDMs showed a similar behavior considering NP accumulation within the edema region like bimodal NP injected animals (Figure 4i and ii). Similarly, for both groups the highest fluorescence intensity within edema region was found 48 h after injection. Control mice receiving nonfluorescent NPs or NaCl solution showed no specific NIRF-signaling in the edema region. These data suggest the accumulation and NIR-detectability of labeled NPs in edema regions of mice indicating the applicability for intraoperative NIRF-imaging.

Revealing long-term *in vivo* biodistribution of fluorescent NPs in mice the fluorescence signal of inflammation was well detectable up to 1 week p.i. In contrast, 12 weeks p.i. edema fluorescence signal was on the same level as it was at every time point for nonfluorescent NP- and NaCl-treated animals (Figure 4).

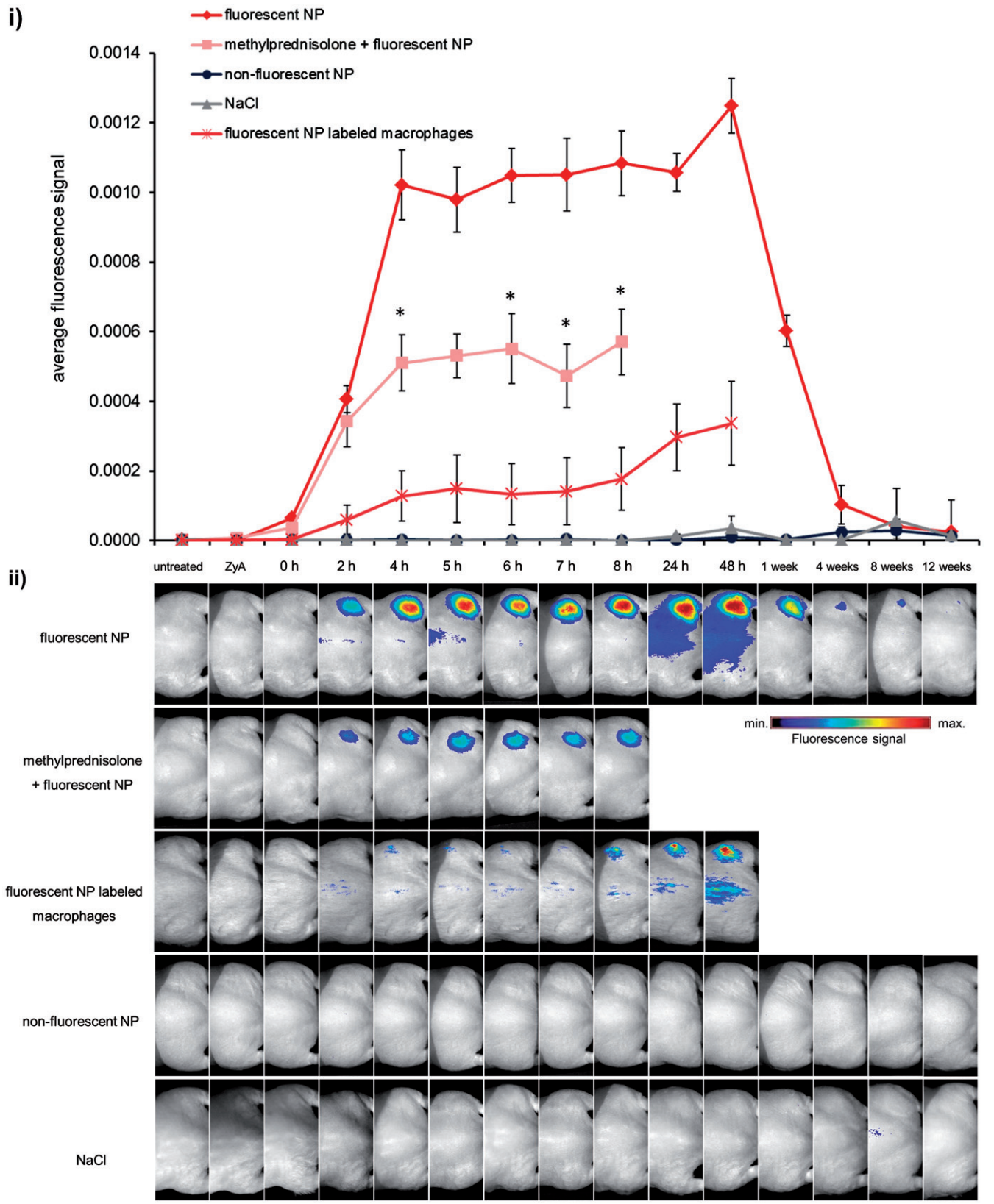

Figure 4. Optical imaging of mononuclear phagocytic cells in hind leg edema with fluorescent NPs in NMRI-mice. Edema was induced subcutaneously at right hind leg using 1% zymosan A solution. NaCl-solution injected *s.c.* at left hind leg served as a control for edema development. Edema-bearing mice were injected i.v. with fluorescent NPs (40 µmol Fe/kg bw) showing an increasing NIRF-signal within edema region starting from 2 h up to a maximum at 48 h after NP-injection. Nonfluorescent NPs and NaCl solution served as a control for specific edema signaling exhibiting no fluorescence within the inflammable region. To confirm NP uptake in mononuclear phagocytic cells mice were treated with methylprednisolone leading to about half of the fluorescence intensity in the edema region compared to the group without treatment. *$p< 0.05$. A further group of mice was injected with fluorescent NP-labeled macrophages which were accumulating within the area of edema region similarly to the bimodal NPs. (i) Semi-quantitative analysis of NIRF-signals in edema region after i.v. injection and (ii) intensity scaled NIRF-images of mice abdomen exhibiting fluorescently-labeled cells of the MPS within edema region.

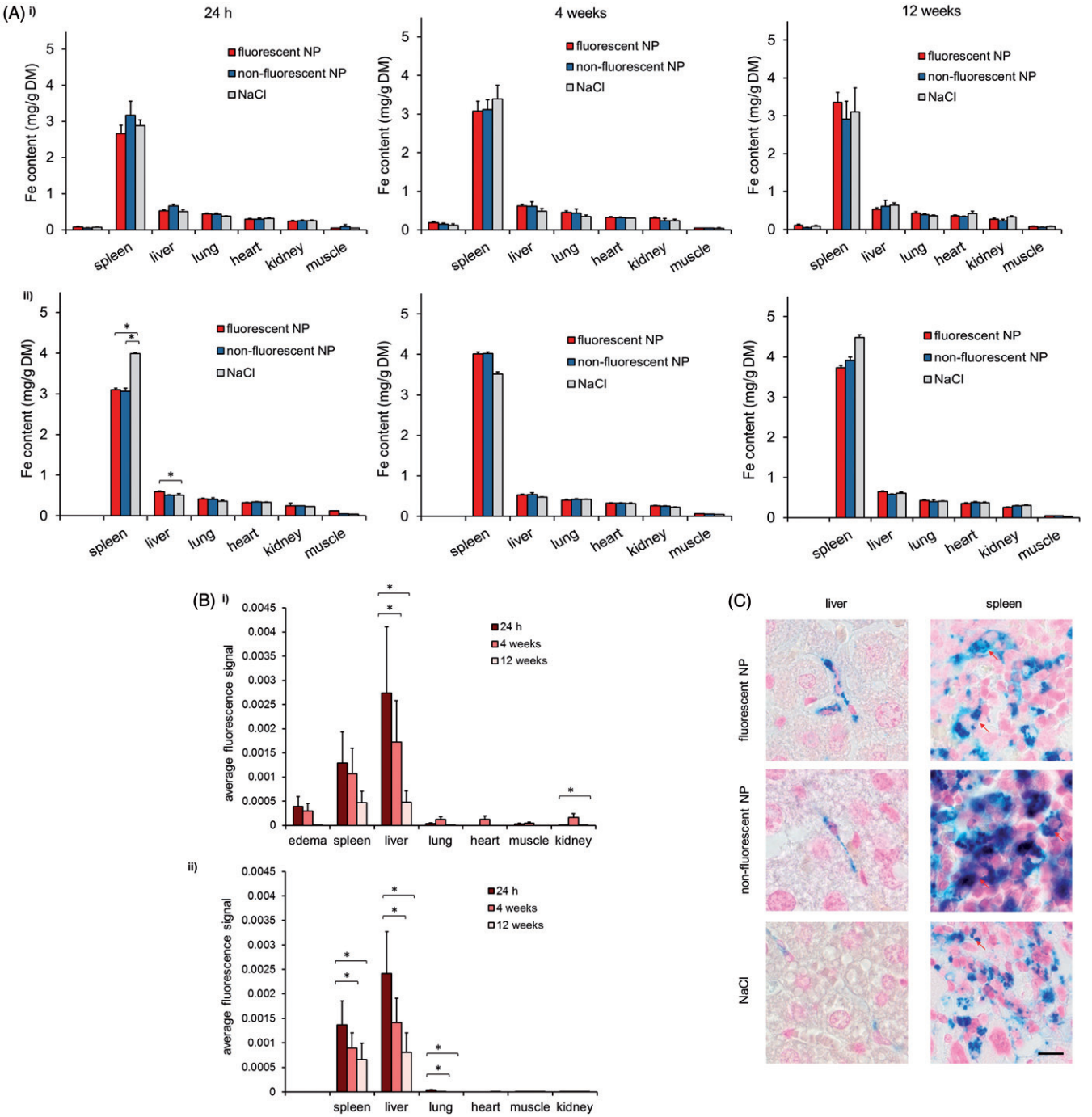

Figure 5. Systemic biodistribution of fluorescent NPs in NMRI-mice. Edema bearing and healthy mice were injected i.v. with fluorescent NPs (40 µmol Fe/kg bw). For each group control mice received unlabeled NPs or NaCl solution instead. (A) Quantification of Fe-content in edema and mice organs of (i) edema bearing mice (ii) or healthy mice 24 h, 4 and 12 weeks after application of NPs. (B) Analysis of fluorescent NP biodistribution in NMRI-mice with a NIRF small animal scanner. Fluorescence intensity of edema and various organs of (i) edema bearing (ii) and healthy mice *ex vivo*. (C) Histological analysis of tissues by Prussian blue staining 24 h after application of fluorescent NPs in edema-bearing mice. Representative organs, hosting cells of the MPS (liver and spleen) are shown compared to the unlabeled NP pendant and NaCl-treated control mice. Red arrows indicate Fe^{3+} located within cells. Scale bar: 10 µm.

These findings indicate prolonged retention time of fluorescent NPs within edema region but also degradability of NPs over time allowing long-term labeling of inflammation processes and flexible surgery planning.

Accumulation of bimodal NPs in mouse organs hosting cells of the MPS

The *ex vivo* examination of long-term distribution in organs of mice showed a preferred accumulation of fluorescence labeled NPs within organs hosting cells of the MPS (liver, spleen, lung, etc.) regardless of the animals' state of health (Figure 5A and B). In general, after application of fluorescently labeled NPs, the highest fluorescence signal was achieved at 24 h after injection (organs, edema; Figure 5B). Later on, NIRF signal decreased constantly over time in edema, liver and lung, whereas the spleen revealed only a slight reduction of fluorescence signal. A complete abolition of fluorescence signals was not visible over the whole observation time of 12 weeks (see also Data S1, Supplementary material). Compared to organs of the MPS,

muscle, heart and kidney showed no or only minor fluorescence signals.

The fate of the metallic component of the NPs in organ tissues revealed a preferential accumulation of iron in the spleen (Figure 5A, Data S2, Supplementary material). Obviously, this finding was independent of the presence of the fluorophore on the NPs indicating that NP-labeling with IR780 does not affect biodistribution of the NPs regarding healthy as well as edema bearing animals (Figure 5A). With consideration of the comparative effects in healthy versus diseased animals, lower iron contents were detected, in tendency, in organs of diseased animals (Data S2, Supplementary material). These findings indicate that the state of health per se also influences iron accumulation or homeostasis within organs hosting cells of the MPS.

Histological analyses of MPS-hosting organs of edema bearing mice showed that NPs were preferentially localized in blood vessels within liver tissue (24 h p.i., Figure 5C). NPs were either located extracellularly or around the nuclei after uptake into phagocytic cells. A strong iron accumulation was seen in cells being located in the red pulp of the spleen of all animals; this effect was independent from the application of NPs to the animals.

Impact of NP application on serum transferrin level in edema bearing and healthy mice

The investigations of the impact of the NP injection on the transferrin levels in blood revealed overall no significant changes (compare NP-treated with NaCl-treated mice) regardless of state of health and time point after application (Data S3, Supplementary material).

Discussion

Our innovative bimodal starch-coated NPs were able to detect murine macrophages *in vitro* and *in vivo* under conditions of inflammation using MRI and NIRF optical imaging. Besides their nontoxic behavior on phagocytes the fluorescent NPs did not differ in terms of physicochemical properties, *in vivo* organ biodistribution and influence on transferrin level from the unlabeled NP pendant.

The *in vitro*-characterization of fluorescence-labeled NPs demonstrated that labeling with the lipophilic dye did not lead to modifications in physicochemical behavior of the NPs in comparison to the unlabeled control. Hence, the suggested starch coating strategy leads to stable NPs successfully shielding the lipophilic fluorescence dye and iron oxide from environmental interactions, such as the adsorption of a protein corona to the particles (Cho et al., 2011).

From the MR imaging point of view, fluorescently labeled and nonlabeled particles showed similar potential with respect to T_2-shortening after NP incubation on macrophages. However, the slightly higher relaxivities of nonfluorescent NPs compared to fluorescently labeled NPs after uptake into the cells can be explained by the presence of the dye, which is located below the shell of these NPs. It is conceivable that the NIR-dye which surrounds the magnetic core in addition to the starch-matrix decreases interactions between magnetite and water protons from the environment. Thus, the influence of fluctuating local dipole-fields on proton relaxation might be decreased due to the additional NIR-dye. This would finally be responsible for the slightly minor shortening of the transverse relaxation times which is nevertheless acceptable for diagnostic MR-screening.

A strong uptake of fluorescence labeled NPs into macrophages and accumulation around the nuclei of the cells was detected suggesting cytoplasmic localization of the starch-coated NPs and uptake via phagocytotic or endocytotic mechanisms. In this context, the presence of the NIR-dye did not alter internalization into macrophages and starch coating led to complete shielding of this dye. Both particles were neutral with a hydrodynamic diameter of about 130 nm.

The investigation of the metabolic effects of our bimodal NPs on the cellular ATP-level of macrophages unveiled no harmful effects. Obviously, labeling with IR780 does not affect cell viability. Thus, the magnetic core and IR780-dye are stable and suitable for imaging conditions and cellular applications. The fluorescent dye is successfully shielded from interactions with inner cell compartments.

Our data on oxidative impact on macrophages indicated that the presence of both the dye and the NPs per se did not enhance the production of ROS in J774A.1-cells. Thus, fluorescence dye labeling did not affect the production of ROS in those cells. Knowing that significantly higher ROS production is expected to be produced by macrophages as a consequence of pathogen contact like protozoa or bacteria, we conclude that recognition and uptake of our NPs will not activate ROS-mediated pathways, such as cellular injury in the form of damaged DNA, lipids and proteins (Channon et al., 1984; Marcato et al., 2008). In contrast, there are indications that some nanomaterials can induce intracellular ROS production which can further lead to higher cytotoxic effects or cell death (Gaspar et al., 1992; Lunov et al., 2011; Naha et al., 2010, Ott et al., 2007). This was not the case for our bimodal NPs. Neither increasing ROS-levels nor cytotoxic effects were observed, making the particles suitable for *in vivo*-applications such as diagnosis and intraoperative imaging.

In vivo studies demonstrated the accumulation of the 134 nm bimodal NPs in zymosan A induced hind leg edema regions of mice by MRI and optical imaging. Observing strong and continuous accumulation of bimodal NPs in edema up to 48 h after i.v. application, we conclude that NPs are taken up by cells of the MPS, which are then migrating and accumulating in the region of inflammation. In this context, monocytes migrate from the blood to the site of inflammation and differentiate into macrophages and after 12–24 h macrophages become the predominant histologic feature of the inflammatory infiltrate (Issekutz & Issekutz, 1993). Hence, migration of NP-loaded macrophages to the edema region allows visualization of the inflammable process.

MRI studies revealed that NP accumulation within mononuclear cells migrating to the inflammation resulted in a clear discrimination between cyst of edema and inner pus and proteinous liquid embedding the edema. In addition, the enhanced NIRF signaling of edema 4–48 h after NP injection was in agreement with data from Ajuebor et al. (1998) showing that monocytes and macrophages are attracted to the site of the zymosan A injection in a peritonitis model with steadily increasing recruitment of cells between 6 and 24 h. Thus, we conclude that infiltration of NP-labeled cells into edema region occurs up to 48 h after injection. These assumptions were strongly supported by our findings of a similar progress in fluorescence detection after injection of bimodal NP-labeled BMDMs into edema bearing NMRI mice. Injection of these cells also resulted in a maximum fluorescence signal after 48 h, which confirms the specific migration of NP-labeled macrophages to the inflammation site. The specific infiltration of phagocytes to the site of edema could be also verified by the application of methylprednisolone. In edema regions of methylprednisolone-treated mice, accumulation of bimodal NPs was observed to be significantly decreased in comparison to mice with no treatment. Due to its gene regulatory impact after binding to intracellular soluble glucocorticoid receptors, the application of methylprednisolone leads to a reduction of the inflammatory cytokine cascade (Sloka & Stefanelli, 2005). Finally, this results in a diminished recruitment rate of phagocytes from the blood stream to the edema

region and to a minor fluorescence signal. Together with the observed *in vivo* MR signals of the bimodal NPs in the edema region, the fluorescence-detectability of the NPs underlines their stability, which allows detection of edema and individual long time planning for intraoperative surgery. Due to the comparable low amount of iron oxide (40 µmol Fe/kg body weight) applied to the mice which is close to the concentrations used for clinically approved iron oxide based MRI-contrast agents like Resovist® (5.8–12.9 µmol Fe/kg body weight), we propose that our NPs will be able to detect edema by imaging cells of the MPS in larger mammals and even humans. Due to the fact that the metabolic rate in large-bodied animals and humans is slower than in small animals like mice, fluorescence of the NPs will expectedly maintain long enough and remain sufficient to detect the NPs for NIRF-guided surgery also in larger biological systems. However, for human applications the NP-dosage has to be evaluated and adapted carefully (clinical trials). Overall, the successful labeling of cells of the MPS by fluorescence labeled NPs and detection via MRI and fluorescence imaging promises the use of these particles as a bimodal contrast agent suitable for T_2-weighted preoperative MR diagnostics and intraoperative NIRF-optical imaging of inflammation.

Investigations on *ex vivo* organ biodistribution of bimodal NPs revealed well detectable fluorescence signals in organs hosting cells of the MPS, especially for liver and spleen showing that NP-loaded cells were accumulating these particles there. The fact that the NP labeling with NIR-dye did not affect NP biodistribution in edematous and healthy mice confirms that the bimodal NP formulation is stable and NIR-dye is successfully shielded by starch coating in both physiological stages. However, decreasing fluorescence signals over time in organs of the MPS suggest that these NPs were degradable. These characteristics of the bimodal NPs show that they fulfil important conditions for the application as a contrast agent.

Interestingly, NP biodistribution was independent of the animals' state of health (edematous and healthy animals). These findings lead to the conclusion that NP accumulation or organ distribution per se is not primarily altered due to the inflammation process. In contrast to that, iron homeostasis was observed to be changed if an inflammation process (edema) has been induced. The fact that the health state can alter biodistribution of biomaterials has already been shown for NIR-dye labeled antibody probes in a model for antigen induced arthritis (Dietzel et al., 2013). In general, we observed that the splenic iron level in edema bearing mice tends to be lower than in healthy mice, which was most likely due to inflammation and its influence on iron homeostasis. This effect might well be due to reduced iron absorption and recycling of senescent erythrocytes in macrophages during inflammation: Hepcidin, the main iron regulatory hormone, which is secreted by hepatocytes, binds to ferroportin on macrophages and triggers its internalization and lysosomal degradation which finally leads to prevention of iron recycling (Munoz et al., 2009). In contrast to that the healthy spleen has a normal iron recycling state by cells of the MPS. Thus, degradation of nanoparticular iron oxide after intravenous application might be also changed in the case of inflammation.

In comparison, by injecting a low dose of iron oxide NPs (1 µmol Fe/25 g bw), which follows distribution through the whole body the detected alterations in iron level primarily result from redistribution of intrinsic iron. Thus, the more sensitive fluorescence data reflect NP-accumulation and degradation more confidently. Consequently, edema induction did not influence NP organ biodistribution per se but might alter abundance of NPs within these organs and intrinsic iron levels. Thus, the application of our bimodal NPs as pre- and intraoperative contrast agents can be considered as uncritical as degradation takes place over time in healthy organisms as well as in a system of inflammation.

Biocompatibility and degradability of NPs were also verified by our histological findings indicating that Fe^{3+} was not detected within hepatic cells but only extracellularly and within intrasinusoidally located cells (possibly phagocytes). Furthermore, splenic tissue revealed that the red pulp contained phagocytic cells which had internalized or were surrounded by accumulated Fe^{3+}, especially after NP-application. We suggest that NP degradation takes place within these cells. These observations demonstrated that no persistent iron accumulation occurs within these tissues and emphasizes once more the proper *in vivo* applicability of our NPs. Irrespective of that, the similar localization of IR780-labeled and unlabeled NP counterparts within phagocytic cells show that the NIR-dye labeling did not alter biodistribution of the NPs on a cellular level representing once more the stability of our fluorescent NP construct for probable pre- and intraoperative imaging.

Further positive aspects arguing for the application of our bimodal NPs were demonstrated by the investigations that neither NP treatment nor inflammation had an impact on serum transferrin level after 24 h to 12 weeks of NP application. These findings support our assumptions that the applied iron oxide concentration was comparatively low and did not alter transferrin level even in the case of inflammation demonstrating good biocompatibility. Furthermore, the entirely starch-coated NPs are taken up by phagocytic cells within a few min after i.v. injection, thus NP iron oxide is not available immediately to alter transferrin levels. However, transferrin levels are known to be changed due to inflammation leading to hypoferremia for several hours (Constante et al., 2007). Based on our investigations that no alterations of transferrin levels were observed 24 h after edema initiation, we conclude that according changes take place shortly after initiation of inflammation but are not influenced by NP injection (see above). Thus, NP application had no lasting effect on serum transferrin level regardless of the inflammation processes and NIR-dye labeling. Therefore, our bimodal NPs fulfil important preconditions for their application as pre- and intraoperative contrast agent by being well-tolerable under healthy but also inflammable conditions. Thus, our bimodal NPs are feasible tools for the visualization of chronic inflammable disorders of the gastrointestinal tract like IBD.

Conclusion

In summary, we demonstrated the successful enhancement of T_2-weighted MR-imaging and the NIRF-detectability of the innovative and biocompatible fluorescent NPs after accumulation within phagocytes and edema regions. This indicates that these NPs might be appropriate for pre- and intraoperative imaging of inflammation. Moreover, the adequate retention time within inflamed tissue (edema) and on the other hand degradability of the NPs in cells of the MPS makes them very suitable for flexible operation planning and medical application.

Interestingly, the application of iron oxide-based NPs might basically impact biodistribution or degradation of nanoparticular and intrinsic iron, potentially leading to slight changes in iron homeostasis in presence of inflammation. Taken together, the simple structure of NIR-fluorochrome-labeled NPs makes them very suitable as a biocompatible and useful tool for *in vivo* preoperative MR- and intraoperative optical imaging of inflammation.

Acknowledgements

We gratefully acknowledge Andreas Kalytta-Mewes and Prof. Dr Dirk Volkmer (University of Augsburg, Institute of Physics, Chair of Solid State Chemistry) for performing BET-measurement. We thank Katja

Haedicke and Doreen May for technical assistance during the mice edema studies and Julia Göring for the treatment and histological staining of mice organs. We would also like to thank Martin Böttcher (University Hospital Jena, Institute for Immunology) for valuable tips concerning ELISA studies and *in vivo* investigations. Furthermore, we are grateful to Prof. Dr Biskup (University Hospital Jena, Group Biomolecular Biophotonics) and Florian Schlenk (University Jena, Faculty of Biology and Pharmacy) for supporting the performance on photon correlation spectroscopy and zeta potential measurements.

Declaration of interest

The authors report no conflict of interest. The authors alone are responsible for the content and writing of the paper. Support of the Bundesministerium für Bildung und Forschung (BMBF) is gratefully acknowledged (project NanoMed).

References

Ajuebor MN, Flower RJ, Hannon R, Christie M, Bowers K, Verity A, Perretti M. 1998. Endogenous monocyte chemoattractant protein-1 recruits monocytes in the zymosan peritonitis model. J Leukoc Biol 63: 108–16.

Channon JY, Roberts MB, Blackwell JM. 1984. A study of the differential respiratory burst activity elicited by promastigotes and amastigotes of *Leishmania donovani* in murine resident peritoneal macrophages. Immunology 53:345–55.

Chen W, Jarzyna PA, Van Tilborg GA, Nguyen VA, Cormode DP, Klink A, et al. 2010. RGD peptide functionalized and reconstituted high-density lipoprotein nanoparticles as a versatile and multimodal tumor targeting molecular imaging probe. FASEB J 24:1689–99.

Cheng L, Yang K, Li Y, Zeng X, Shao M, Lee ST, Liu Z. 2012. Multifunctional nanoparticles for upconversion luminescence/MR multimodal imaging and magnetically targeted photothermal therapy. Biomaterials 33:2215–22.

Cho EC, Zhang Q, Xia Y. 2011. The effect of sedimentation and diffusion on cellular uptake of gold nanoparticles. Nat Nanotechnol 6:385–91.

Constante M, Wang D, Santos MM. 2007. Repression of repulsive guidance molecule C during inflammation is independent of HFE and involves tumor necrosis factor-alpha. Am J Hematol 82:549.

Cummings SA, Rubin DT. 2006. The complexity and challenges of genetic counseling and testing for inflammatory bowel disease. J Genet Couns 15:465–76.

Dietzel F, Boettger MK, Dahlke K, Holzer J, Lehmann F, Gajda M, et al. 2013. Assessment of rat antigen-induced arthritis and its suppression during glucocorticoid therapy by use of hemicyanine dye probes with different molecular weight in near-infrared fluorescence optical imaging. Invest Radiol 48:729–37.

Gaspar R, Preat V, Opperdoes FR, Roland M. 1992. Macrophage activation by polymeric nanoparticles of polyalkylcyanoacrylates – activity against intracellular *Leishmania-donovani* associated with hydrogen-peroxide production. Pharm Res 9:782–7.

Hoskins C, Wang L, Cheng WP, Cuschieri A. 2012. Dilemmas in the reliable estimation of the *in-vitro* cell viability in magnetic nanoparticle engineering: which tests and what protocols? Nanoscale Res Lett 7:77.

Issekutz AC, Issekutz TB. 1993. Quantitation and kinetics of blood monocyte migration to acute inflammatory reactions, and IL-1 alpha, tumor necrosis factor-alpha, and IFN-gamma. J Immunol 151:2105–15.

Jaffer FA, Libby P, Weissleder R. 2009. Optical and multimodality molecular imaging: insights into atherosclerosis. Arterioscler Thromb Vasc Biol 29:1017–24.

Jarrett BR, Gustafsson B, Kukis DL, Louie AY. 2008. Synthesis of 64Cu-labeled magnetic nanoparticles for multimodal imaging. Bioconjug Chem 19:1496–504.

Khatami M. 2009. Inflammation, aging, and cancer: tumoricidal versus tumorigenesis of immunity: a common denominator mapping chronic diseases. Cell Biochem Biophys 55:55–79.

Koktysh D, Bright V, Pham W. 2011. Fluorescent magnetic hybrid nanoprobe for multimodal bioimaging. Nanotechnology 22:275606.

Lee YD, Lim CK, Singh A, Koh J, Kim J, Kwon IC, Kim S. 2012. Dye/peroxalate aggregated nanoparticles with enhanced and tunable chemiluminescence for biomedical imaging of hydrogen peroxide. ACS Nano 6:6759–66.

Lunov O, Syrovets T, Loos C, Nienhaus GU, Mailander V, Landfester K, et al. 2011. Amino-functionalized polystyrene nanoparticles activate the NLRP3 inflammasome in human macrophages. ACS Nano 5: 9648–57.

Mackay PS, Kremers GJ, Kobukai S, Cobb JG, Kuley A, Rosenthal SJ, et al. 2011. Multimodal imaging of dendritic cells using a novel hybrid magneto-optical nanoprobe. Nanomedicine 7:489–96.

Marcato LG, Ferlini AP, Bonfim RC, Ramos-Jorge ML, Ropert C, Afonso LF, et al. 2008. The role of Toll-like receptors 2 and 4 on reactive oxygen species and nitric oxide production by macrophage cells stimulated with root canal pathogens. Oral Microbiol Immunol 23: 353–9.

Munoz M, Villar I, Garcia-Erce JA. 2009. An update on iron physiology. World J Gastroenterol 15:4617–26.

Naha PC, Davoren M, Lyng FM, Byrne HJ. 2010. Reactive oxygen species (ROS) induced cytokine production and cytotoxicity of PAMAM dendrimers in J774A.1 cells. Toxicol Appl Pharmacol 246: 91–9.

Nahrendorf M, Jaffer FA, Kelly KA, Sosnovik DE, Aikawa E, Libby P, Weissleder R. 2006. Noninvasive vascular cell adhesion molecule-1 imaging identifies inflammatory activation of cells in atherosclerosis. Circulation 114:1504–11.

Ott M, Gogvadze V, Orrenius S, Zhivotovsky B. 2007. Mitochondria, oxidative stress and cell death. Apoptosis 12:913–22.

Philip M, Rowley DA, Schreiber H. 2004. Inflammation as a tumor promoter in cancer induction. Semin Cancer Biol 14:433–9.

Radermacher KA, Beghein N, Boutry S, Laurent S, Elst LV, Muller RN, et al. 2009. *In vivo* detection of inflammation using pegylated iron oxide particles targeted at E-selectin a multimodal approach using MR imaging and EPR spectroscopy. Invest Radiol 44:398–404.

Rimkus G, Bremer-Streck S, Gruttner C, Kaiser WA, Hilger I. 2011. Can we accurately quantify nanoparticle associated proteins when constructing high-affinity MRI molecular imaging probes? Contrast Media Mol Imaging 6:119–25.

Rimkus G, Gruttner C, Bremer-Streck S, Herrmann KH, Krumbein I, Reichenbach JR, et al. 2012. mVCAM-1 specific iron oxide nanoparticles based probes for multimodal imaging purposes. Biomed Tech (Berl) 57:77–88.

Schwartsburd PM. 2003. Chronic inflammation as inductor of pro-cancer microenvironment: pathogenesis of dysregulated feedback control. Cancer Metastasis Rev 22:95–102.

Sharma P, Bengtsson NE, Walter GA, Sohn HB, Zhou G, Iwakuma N, et al. 2012. Gadolinium-doped silica nanoparticles encapsulating indocyanine green for near infrared and magnetic resonance imaging. Small 8:2756–68.

Sloka JS, Stefanelli M. 2005. The mechanism of action of methylprednisolone in the treatment of multiple sclerosis. Mult Scler 11:425–32.

Stoll G, Basse-Lusebrink T, Weise G, Jakob P. 2012. Visualization of inflammation using (19) F-magnetic resonance imaging and perfluorocarbons. Wiley Interdiscip Rev Nanomed Nanobiotechnol 4:438–47.

Tsourkas A, Shinde-Patil VR, Kelly KA, Patel P, Wolley A, Allport JR, Weissleder R. 2005. *In vivo* imaging of activated endothelium using an anti-VCAM-1 magnetooptical probe. Bioconjug Chem 16:576–81.

Yang K, Hu L, Ma X, Ye S, Cheng L, Shi X, et al. 2012. Multimodal imaging guided photothermal therapy using functionalized graphene nanosheets anchored with magnetic nanoparticles. Adv Mater 24: 1868–72.

Supplementary material available online
Supplementary Figures 1–3.